

Dynamic mesh analysis by numerical simulation of internal combustion engines

<http://dx.doi.org/10.1590/0370-44672023770003>

José Antônio da Silva^{1,5}

<https://orcid.org/0000-0003-4813-1029>

Lucas Pereira da Silva^{2,6}

<https://orcid.org/0000-0001-6365-1984>

Júlio César Costa Campos^{2,7}

<https://orcid.org/0000-0002-9488-8164>

Antônio Marcos de Oliveira Siqueira^{3,8}

<https://orcid.org/0000-0001-9334-0394>

Alexandre Gurgel^{3,9}

<https://orcid.org/0000-0002-3120-8168>

Luben Cabezas Gómez^{4,10}

<https://orcid.org/0000-0002-9550-9453>

¹Universidade Federal de São João del-Rei – UFSJ,
Departamento de Ciências Térmicas e dos Fluidos,
São João del-Rei – Minas Gerais - Brasil.

²Universidade Federal de Viçosa – UFV,
Centro de Ciências Exatas e Tecnológicas,
Departamento de Engenharia de Produção e Mecânica,
Viçosa - Minas Gerais - Brasil.

³Universidade Federal de Viçosa – UFV,
Centro de Ciências Exatas e Tecnológicas,
Departamento de Química,
Viçosa - Minas Gerais – Brasil.

⁴Universidade de São Paulo - USP,
Escola de Engenharia de São Carlos,
Departamento de Engenharia Mecânica,
São Carlos – São Paulo – Brasil.

E-mails: ⁵jant@ufsj.edu.br, ⁶lucas.p.pereira@ufv.br,
⁷julio.campos@ufv.br, ⁸antonio.siqueira@ufv.br,
⁹agurgel@ufv.br, ¹⁰lubencg@sc.usp.br

Abstract

A continuous increase in levels of atmospheric pollution and emission restrictions has forced scientists and engineers to adopt new strategies to improve and develop internal combustion engines. One strategy is based on the development of new simulation methodologies using computational fluid dynamic (CFD) techniques, proposed in the present article. In this study, the dynamic loop methodology with ANSYS Fluent code is proposed to perform the numerical simulation of a four-stroke spark ignition engine. The complexity of the real case was first simplified with three-dimensional CAD geometry, which was then discretized in ANSYS Meshing, whereby a hybrid mesh was created using prismatic and tetrahedral elements. Simulations for in-cylinder analyses were performed in cold flow and employing common flow parameters, such as swirl and tumble. The mesh quality results were classified as good or excellent, being higher than 0.79 for orthogonal quality criteria and lower than 0.36 for skewness criteria. Turbulent effects were introduced concerning the opening and closing of the valves. It was found that the turbulence increases during the intake stroke up to 90°, and during the power stroke, wherein the of the piston bowl, had a great contribution that can be seen from the swirl and tumble profile for the engine cycle. In the case of the turbulence intensity, a sharp increase was registered during the admission step up to 90°, at which point the turbulence intensity was 4.0. It can be concluded that this is an innovative approach, capable of simulating the engine motion profile in cold flow.

Keywords: cold flow, dynamic mesh, internal combustion engine, swirl, turbulence intensity.

1. Introduction

A continuous increase in the levels of atmospheric pollution and emission restrictions has forced scientists and engineers to adopt new strategies to improve and develop internal combustion engines (ICE). It is known that, traditionally, the biggest part of the ICE analysis is based on laboratory tests and the construction of countless prototypes, which entail high costs and design time.

However, with the advance of computational technology and improved numerical methods, fields, such as CFD have achieved new levels, to the point of becoming more and more ubiquitous in engineering. This new technique has its utility in the automation of the design processes and reduces costs because of the reduced number of prototypes and physical experiments (Koziel *et al.*, 2016;

Gao *et al.*, 2019). Considering its application to ICE's, CFD is used to numerically solve the governing conservation equations (continuity, momentum, and energy) that describe the physical behavior on a given engine region, still being capable of dealing with the complexity of engine geometry for a wide set of fluid transport processes that occur simultaneously, such as chemical reactions, heat

and mass transfer and high turbulence flows (Gosman, 1999).

Múnera *et al.* (2009), mention in their article that CFD codes are perfectly able to help optimizing internal combustion engines, since they can investigate the geometric details of such equipment. In fact, Yogesh *et al.* (2014) argue that this method helps to support the design of parts for the engine geometry and physical parameters by using parameters like magnitude contours and three-dimensional visualization of the requested variables for each time of the process, so as to devise an engine with the most perfect working conditions. This support can be, for example, the analyses of the turbulence effects for different types of pistons (Yin *et al.*, 2016), investigations on modifications in the connecting rod length (Zunaid *et al.*, 2017), studies on combustion effects (Islam *et al.*, 2016), or even some insights about the influence of piston bowl geometry and the fuel conditions on the resonance of these

engines (Broatch *et al.*, 2007).

Also, Gafoor & Gupta (2015), demonstrated the influence of a piston bowl in generating vorticities employing the swirl ratio in their numerical investigation, which is one of the main search parameters of the combustion quality and air-fuel mixture (Priscilla & Meena, 2013).

It is also important to provide a good mesh generation; that is, a mesh that is perfectly capable of representing the physical domain. In the case of ICE simulations and according to Junior (2010), it is necessary to have a mesh that can expand by adding cells and contract by removing cells axially in time, to enable the simulation of piston and valves motion. This process is important because it accommodates the geometry changes during the different time steps, and it does that by moving the mesh nodes while the node's connectivity can initially be kept unchanged (He *et al.*, 2019).

This kind of mesh is known as dy-

namic mesh. In the studies of Shafie & Said (2017), and Rohith & Prakash (2015), the development of turbulent effects in ICE's was verified for cold flow simulations using dynamic meshes. The simulations were performed using the Ansys Fluent code and the results are very satisfactory, demonstrating the utility of this type of mesh for the particular case of ICEs.

Therefore, the present study has the aim of evaluating the operation and use of dynamic meshes for ICE simulations as a mechanism to improve their efficiency. More specifically, simulated are the hydrodynamics and turbulence of a cold flow in an assembly formed by cylinder-piston, and intake and exhaust valves and ports of a four-stroke ICE. The study focuses on the description of the flow field variation with piston and valve movements, including the analysis of flow turbulence behavior and their influence on macroscopic parameters as swirl and tumble ratios, respectively.

2. Theoretical considerations

2.1 Mathematical model

The cold flow simulation deals with the air flow modeling in the engine under transient, non-isothermal conditions with no chemical reactions in the processes,

which allows to study the air fuel mixture and its interaction with the geometry chamber (Rohith & Prakash, 2015).

The RANS approach to turbulence

modeling requires that the Reynolds stresses are appropriately modeled and the Boussinesq hypothesis is employed, Eq. (1).

$$-\rho \overline{u'_i u'_j} = \mu_t \left(\frac{\partial u_i}{\partial x_j} + \frac{\partial u_j}{\partial x_i} \right) - \frac{2}{3} \left(\rho k + \mu_t \frac{\partial u_k}{\partial x_k} \right) \delta_{ij} \quad (1)$$

The governing equations of continuity, momentum, energy and k-epsilon

RNG model are indicated below, Eq. (2), Eq. (3), Eq. (4), Eq. (5) and Eq. (6).

$$\frac{\partial \rho}{\partial t} + \nabla \cdot (\rho \cdot \vec{v}) = 0 \quad (2)$$

$$\frac{\partial \rho}{\partial t} (\rho \vec{v}) + \nabla \cdot (\rho \vec{v} \vec{v}) = \nabla p + \nabla \cdot (\vec{\tau}) \quad (3)$$

$$\frac{\partial}{\partial t} (\rho H) + \nabla \cdot (\rho \vec{v} H) = \nabla \cdot \left(\frac{k_t}{c_p} \nabla H \right) \quad (4)$$

$$\frac{\partial}{\partial t} (\rho k) + \frac{\partial}{\partial x_i} (\rho k u_i) = \frac{\partial}{\partial x_i} \left(\alpha_k \mu_{eff} \frac{\partial k}{\partial x_i} \right) + G_k + G_b - \rho \varepsilon - Y_M \quad (5)$$

$$\frac{\partial}{\partial t} (\rho \varepsilon) + \frac{\partial}{\partial x_i} (\rho \varepsilon u_i) = \frac{\partial}{\partial x_j} \left[\alpha_\varepsilon \mu_{eff} \frac{\partial \varepsilon}{\partial x_j} \right] + C_{1\varepsilon} \frac{\varepsilon}{k} (G_k + C_{3\varepsilon} G_b) - C_{2\varepsilon} \rho \frac{\varepsilon^2}{k} - R_\varepsilon \quad (6)$$

Where μ_t is the turbulent viscosity, ρ is specific mass, v is vector velocity, P is static pressure, $\vec{\tau}$ is stress tensor, I is unit tensor, H is total enthalpy, k is the turbulence kinetic energy, ε is the dissipation rate, u_i is the velocity

component, α_k and α_ε are the inverse effective Prandtl numbers for k and ε , respectively, μ_{eff} is the effective viscosity, G_k is the generated turbulence kinetic energy due to the mean velocity gradients, G_b is the generated turbu-

lence kinetic energy due to buoyancy, Y_M is the fluctuating dilatation in compressible turbulence to the overall dissipation rate, R_ε is a term that depends of k and ε and $C_{1\varepsilon}=1,42$, $C_{2\varepsilon}=1,68$ and (ANSYS Inc. 2013).

2.2 Mesh quality parameters

In ANSYS Meshing, two main criteria were considered to evaluate the mesh quality, namely the orthogonal quality and the skewness. For the orthogonal quality Figure 1, a calculation can be made using Equation 7 to check the cell orthogonality level, with

results ranging from 0 (imperfect cell) to 1 (perfect cell). In Equation 7, \vec{A}_i is the edge normal vector and \vec{f}_i is a vector from the centroid of the face to the centroid of the edge. In the second case, the skewness criteria determine how close to ideal (i.e.,

equilateral or equiangular) a specific face or cell is, where 0 refers to an equilateral cell and 1 indicates a degenerated cell. Also, if the value is less than 0.25, the model is excellent; from 0.25 to 0.50, it is good; from 0.50 to 0.75 it is fair, and above 0.75 it is bad.

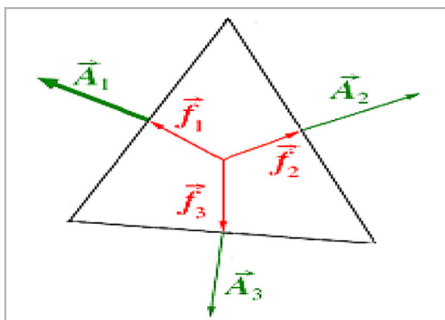


Figure 1 - Orthogonal quality of a cell.

$$y = \frac{\vec{A}_i \cdot \vec{f}_i}{|\vec{A}_i| |\vec{f}_i|} \quad (7)$$

2.3 Turbulent effects

The understanding of the in-cylinder flow motion strongly influences the engine performance (Huang *et al.*, 2005). This turbulent motion is empowered by standards of flow inside the cylinder, such as the swirl, which is a rotational rigid body motion of the airflow that happens around the cylinder vertical axis, and the tumble, which is similar, but has a perpendicular rotation around the cylinder axis (Brunetti, 2012). Both motions follow the right-hand rule.

According to Ferguson (2016), the swirl refers to a large-scale vortex motion into the cylinder and around its long axis, while the tumble refers to a large-scale vortex motion perpendicular to the cylinder axis. They also emphasize that the swirl and tumble approach is the best way to get a fast mixture between air and fuel for direct injection engines. In diesel engines, since the fuel is injected, the swirl bends the fuel jet and convection occurs far from the fuel

injector, thereby providing fresh air for the following fuel upstream.

Numerically, these two parameters are introduced as the swirl ratio (R_s) and tumble ratio (R_t) by Equations 8 and 9, respectively, and represent the ratio between the rotational speed of the fluid and the rotational speed of the engine. Besides that, Shafe & Said (2017) believe that both ratios are the most commonly investigated parameters in fluid dynamics.

$$R_s = \frac{\omega_s \cdot 60}{2\pi N} \quad (8)$$

$$R_t = \frac{\omega_t \cdot 60}{2\pi N} \quad (9)$$

In Equations 8 and 9, N is the engine speed (rpm), ω_s is the angular

speed of the flow mass around the swirl axis, and ω_t is the angular speed

of the flow mass around the tumble axis.

2.4 Dynamic mesh

For (Cong *et al.*, 2020), dynamic meshes are used in systems that have moving edges or fluid zones subjected to some kind of deformation. Moreover, Li *et al.* (2014) advise to use dynamic meshes for getting more accurate predictions about the engine's performance, since this technique is capable of processing complex geometries, hard boundary conditions and properties from the physical variables. ANSYS Fluent also provides three movement methods for the meshes on deformation

edges: smoothing, dynamic layering and remeshing.

The smoothing or mesh deformation method is described by Lin *et al.* (2014) as a nodal repositioning that has the same shape and size of the mesh elements keeping the nodal connectivity, which allows the mesh to accommodate in places that have edge movement and/or deformation without increasing the number of cells. In the case of re-meshing, Lin *et al.* (2014), propose a boundary modification method from

the local or global mesh construction, whereby the flow methods enable fluid properties that are acquired during an interpolation scheme. On the other hand, Blanco & Oro (2012) mention that the dynamic layering is a technique where cells can be created and/or destroyed in agreement with expansion or contraction of the edges. The technique works basically with the addition or reduction of cells, in which case directly changing the topological connectivity of the original mesh.

2.5 Turbulent intensity

The turbulent intensity (TI) is defined by Lam *et al.* (2012), Basse (2019) and

Silva *et al.* (2020) as the ratio between the root mean square (RMS) of the fluctuation

velocity (u') and the mean flow velocity (u_{avg}), as defined by Equation 10.

$$TI = \frac{\sqrt{u'}}{u_{avg}} \quad (10)$$

2.6 Description of numerical simulation methodology

This study focused on performing a numerical simulation of a four-stroke,

internal-combustion engine with piston bowl. The main engine settings can be

found in Table 1.

Table 1 - Engine parameters.

Parameter	Value
Piston diameter	84.00 mm
Connecting rod length	144.3 mm
Crank radius	45 mm
Engine speed	2000 rpm
Compression ratio	10.32
Minimum lift	0.20 mm
Piston offset	0 mm

The complexity of the real model was simplified in a three-dimensional

CAD geometry shown in Figure 2. The geometry was then discretized with

ANSYS by adopting a hybrid mesh, composed of prismatic and tetrahedral elements.

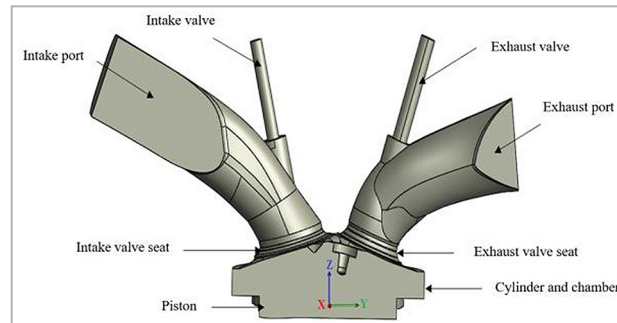


Figure 2 - CAD geometry.

The simulations were performed in cold flow. The engine cycle, having a total cycle of 720° of the crank shaft, was split in 2960 time steps, each one having 0.25°

for the most part of the cycle and 0.125° in some cases, before and after opening and closing the valves. For each time step a total number of 50 iterations was consid-

ered. Figure 3 illustrates the valves motion profile during the entire engine cycle for the engine from Table 1 that also shows the open and closing time of both valves.

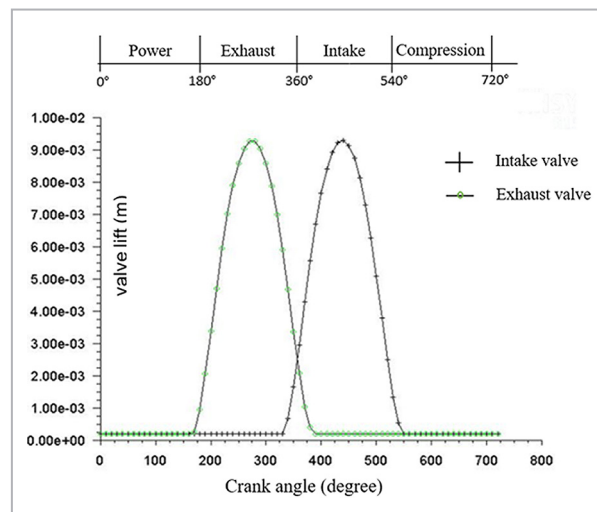


Figure 3 - Valve lift profile.

For the dynamic mesh, the smoothing method was used because of the movement of the valves and piston boundaries. The dynamic layering was considered for adding cells in the piston displacement magnitude and remeshing because of the geometry complexity.

For this simulation, the initial stroke (0°) starts when the engine is powered. In this case, the initial in-cylinder conditions are 1 MPa for static pressure and temperature equal to 593 K.

An inlet and exhaust air temperature of 300 K, pressure of 1 atm and 2% of turbulence intensity were set as the boundary conditions. Also, the hydraulic diameters of 27.009 mm and 22.301 mm were set to inlet and exhaust ports, respectively.

Since it is a non-stationary state simulation, ANSYS Inc. (2013), recommends performing more than one engine cycle to get better results. Thus, 2.5 engine cycles were simulated; that is, the simulation happened from angles 0° to 1800° to the crank, with particular analyses done between the angles of 1080° and 1800° . Besides, for better understanding and easier evaluations about the engine cycles, it was decided to consider the angle of 1080° , as 0° , and 1800° , as 720° , figure 5,6 and 7. That is, from the beginning of admission to the end of exhaust.

Because of the turbulence flow complexity, the turbulence modeling has been and will be a very active search field (Ferguson, 2016). Therefore, the $k-\epsilon$ RNG was used to model the turbulence (Equations 5 and 6).

The pressure-based solver was used to solve the flow solution. For the time discretization, a first-order implicit formulation was chosen. To get a better efficiency for the calculations, the PISO (Pressure implicit with split operators) scheme method was used to couple the velocity (momentum) with the pressure, because the PISO algorithm is capable of drastically minimizing the number of iterations needed to get to the convergence point, especially in non-steady simulations when compared to the SIMPLE and SIMPLEC methods Karthikeyan, and Samuel, (2008).

In ANSYS Fluent, the spatial Green-Gauss Node-Based was chosen for the gradient and the PRESTO! scheme for the pressure. The under-relaxation factors are listed in Table 2.

Table 2 - Under-relaxation factors.

Under-relaxation factor	Value
Pressure	0.3
Momentum	0.5
Density	1.0
Body forces	1.0
Turbulent kinetic energy	0.4
Turbulent viscosity	1.0
Energy	1.0
Turbulent dissipation rate	0.8

The second order upwind scheme was used to interpolate all equations. This choice was justified by Chung (2002), who pointed out that high-order upwind approaches give more accurate results and are

more adequate when the simulations are related to inherently unstable flows (Wang *et al.*, 2007).

Despite this, in some cases, high-order schemes can generate instabilities and even numerical dis-

persion (Junior, 2010). As a result, the combination of first-order and high-order schemes was implemented with the first-order upwind scheme being applied in the interpolation of the turbulent dissipation rate.

3. Results and discussion

3.1 Grid independence test and physical comparison

To keep the agreement between accuracy and computational time, a grid independence test was performed for crank angles from 0° to 15° , to examine

the change in static pressure for three generated meshes, as shown in Figure 4. Then, a quantitative comparison for the crank angle of 15° was made and the results

are shown in Table 3. Mesh 1 was chosen because of the low processing time and considerable accuracy when compared to the other meshes.

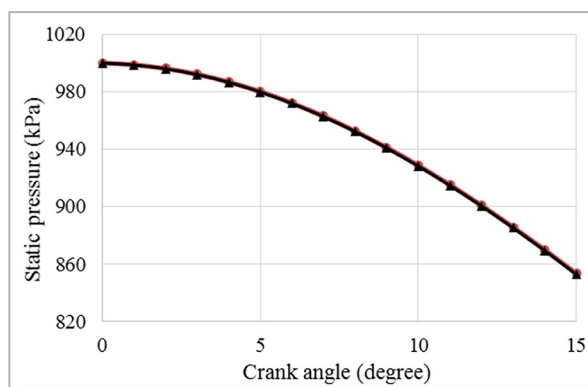


Figure 4 - Static pressure for the three generated meshes.

Table 3 - Grid independence test.

Mesh	Time (h)	Number of Elements (15°)	Static pressure in MPa (15°)
1	1.15	1038075	853944.8639
2	8.17	2507379	853528.4367
3	13.68	5327305	852951.2415

In order to verify the simulated model and the numerical stability of the code, the results were compared with the numerical data presented by (Shafie & Said, 2017). They were checked with the characteristic curve of the static pressure in the engine cylinder as a function of the crankshaft angle, as can be seen in Figure 5.

The agreement was mainly based on the characteristic shape of the curves, although the experiments presented by Shafie & Said (2017) were carried out with the same geometry and in cold flow, but in a different engine.

The authors considered different

parameters for the analyzed engine, such as: engine speed, compression ratio, valve displacement, distance between dead, upper and lower points, and only analyzed part of the cycle, which was 165° to 415°, as shown in Figure 5.

Therefore, it is clear that the authors' curve presents a numerical discrepancy in relation to this study. However, it is noteworthy that even with the different factors involved in the configuration of the engines, the curves presented an average deviation of only 31% between the peak pressures.

It is also noteworthy in relation to the use of the turbulence model used;

that is, Shafie&Said(2017) used the standard k-ε model and this research, the k-ε RNG model.

Briefly, the standard k-ε model has limitations imposed by phenomenological considerations and degrees of empiricism. Differently from the standard k-ε model, the k-ε RNG model presents some refinements capable of providing better precision for tension in fast flows, increasing the precision for flows involving swirl. This model presents analytically derived differential formulation for effective viscosity at low Reynolds numbers and analytical formulation for turbulent Prandtl numbers.

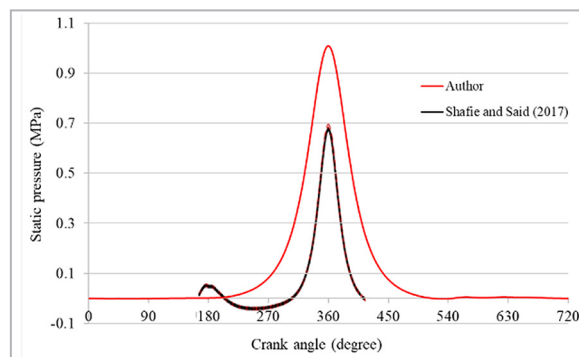


Figure 5 - Static in-cylinder pressure profiles.

3.2 Mesh quality parameters

It is known that proper mesh affects the accuracy of the results when working with numerical experiments and in the simulations of ICE's. However, additional care must be taken in the evaluation of dynamic meshes because they can change over time, therefore their quality parameters also change, which can imply in undesirable

aspects, such as loss of metric qualities, and consequently, poor reliability in the results.

In Figure 6, the orthogonal quality values for all engine working cycles can be seen. It is possible to verify that the parameter changes from 0.79 (minimum value) to 0.90 (maximum value), and the entire cycle has an average orthogonal

quality of 0.86. It is also noticed that the points corresponding to lower-quality numbers, from 300° to 400°, refer to parts of the compression and power strokes. Another fact is that there is no valve lift at this time interval, which is evidence that crushing and stretching of the elements occur, thereby decreasing the orthogonal quality.

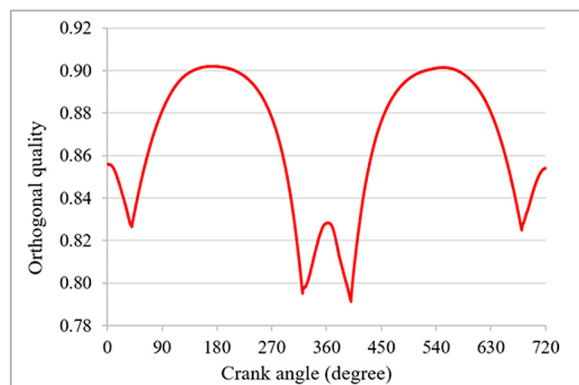


Figure 6 - Orthogonal quality parameter.

Figure 7 shows the same findings of Figure 6 about the lower orthogonal quality points that overcome 0.35

of magnitude. In general, the mesh can be identified as good or excellent in the skewness metric, always

between 0.22 and 0.55, which is very similar to the results from Islam *et al.* (2016).

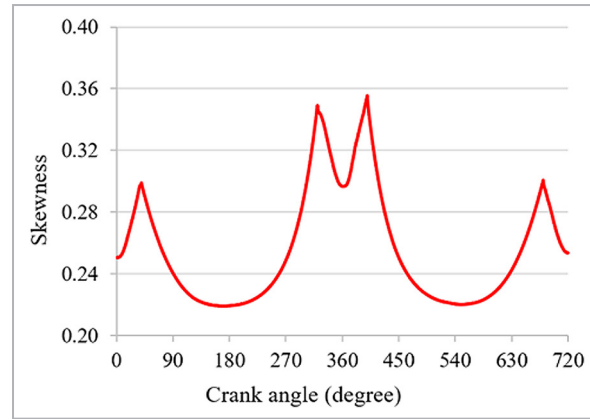


Figure 7 - Skewness parameter.

Another detail is the valve influence in the control volume at the moments when the mesh is created. Based on the fact that the alternative piston movement is always the same, it can be supposed that both orthogonal quality and skewness should keep the same pattern from Figure 7, between

180° and 540°. This however does not happen because of the valve lift from 0° to 180° and from 540° to 720°, according to Figure 3.

Figure 8 shows the accommodation of the created mesh for several time intervals during the engine cycle. These

particular recordings indicate the top dead center, the bottom dead center, and some intermediate points. Specific phenomena occur within defined angle ranges, namely: intake from 0° to 180°, compression from 180° to 360°, power from 360° to 540°, and exhaust from 540° to 720°.

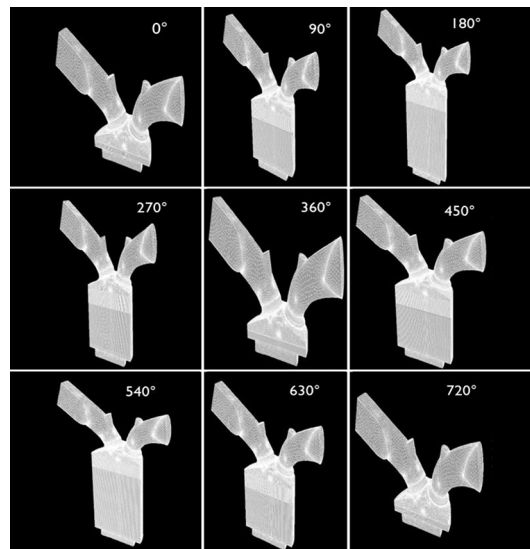


Figure 8 - Dynamic mesh behavior.

Figure 8 highlights the sequence of images that show the increase and

decrease in the number of cells because of the mesh adaptation to the boundary's

displacements. Numerically, these changes can be seen in Figure 9, showing the

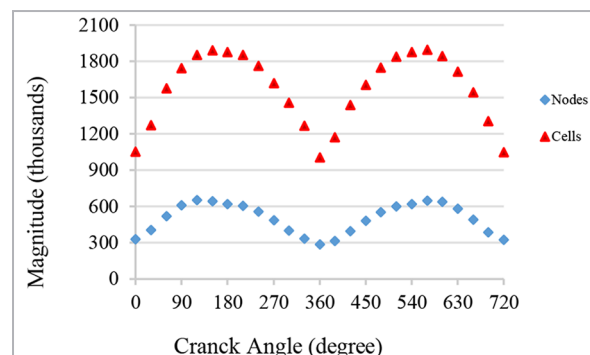


Figure 9 - Number of nodes and cells of the dynamic mesh.

magnitude of the numbers of nodes and cells and their tendency to form a cycle, since the discretized volume has also cyclic characteristics as a function of time, due to the alternative motion of the piston.

Figure 10 shows how the velocity field behaves during the simulation by

the intensity contour technique. From the indicated time steps, it is seen that at 90°, the working flow is pulled into the cylinder in the form of an annular jet because of the high-pressure gradient created when the piston moves directly to the bottom dead center. From this point on, there is

a significant reduction in the jet intensity as a result of an abrupt interaction of the jet with the cylinder walls and the piston surface, increasing turbulence levels, as reported by Junior (2010), and generating similarities with large and small flow scales, according to Ferguson (2016).

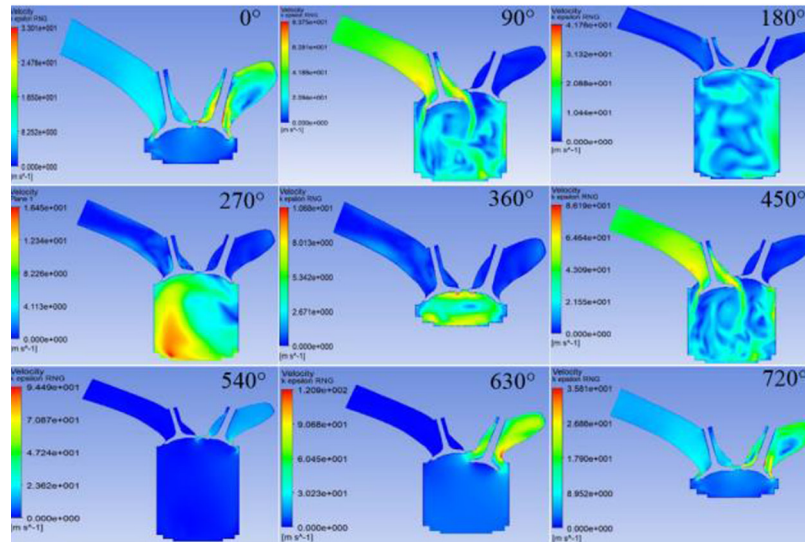


Figure 10 - In-cylinder velocity field.

3.3 Evaluation of turbulent effects

After acquiring good results for the dynamic mesh in each part of the engine cycle, the next step is to verify some of the main physical quantities that affect the performance of the engine strokes, and then to demonstrate the actual usefulness of this novel technique. Figures 11 and 12 show the convergence data for swirl and tumble ratio as a function of crank angle for the discussed case.

In Figure 11, it can be verified that the swirl ratio starts from -0.07 , with a sharp initial increase to a maximum

of -0.33 , as result of the intake valve opening and the flow getting into the cylinder. The negative term actually represents only the motion direction of the swirl. From -0.33 , the swirl ratio decays quickly. Ferguson (2016), justifies this fact as a consequence of dissipative effects from friction, and impact of the fluid jet on the cylinder walls and surface piston. Following this dissipative tendency, the swirl ratio reduces in intensity only at the end of the intake stroke. However the piston bowl works to amplify the intensity

in the compression stroke from 150° to 360°. This similar fact can be seen in the results of Priscilla & Meena (2013); Shafie & Said (2017), who confirmed that the piston bowl works to intensify the turbulent effects.

During the power stroke, from 360° to 540°, the swirl decreases, and at the beginning of the exhaust stroke, in 540°, the piston bowl contributes again to increase the swirl, but this persists up to 650°, and after that, the turbulence decreases until the end of the cycle.

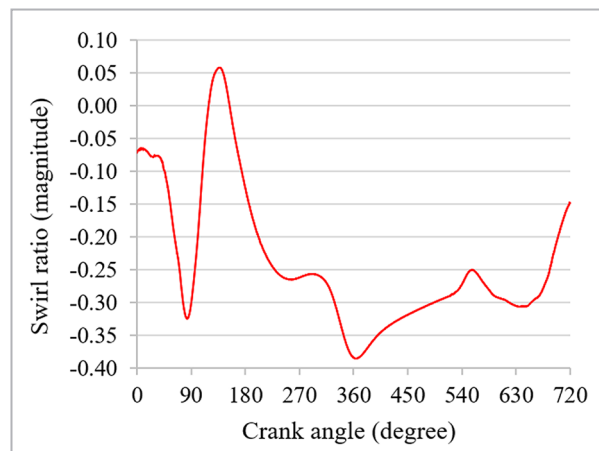


Figure 11 - Swirl ratio.

Figure 12 also shows a considerable increase in tumble ratio during the intake stroke from 0° to 90°, after

which, it starts to decay because of dissipative effects, exactly as described above for the swirl ratio. Nevertheless,

further analysis of Figure 12 indicates that the tumble ratio starts increasing again from 180° and reaches a local

peak at 300°. This magnitude increase suggests again the positive contribution of the piston bowl for increasing the turbulence intensity during the

compression stroke, an effect that is noticed again, but in a small intensity, at the beginning of the exhaust stroke at 540°. This is an expected

event, numerically confirmed by Shafie & Said (2017) and numerically and experimentally by Addepalli & Mallikarjuna (2018).

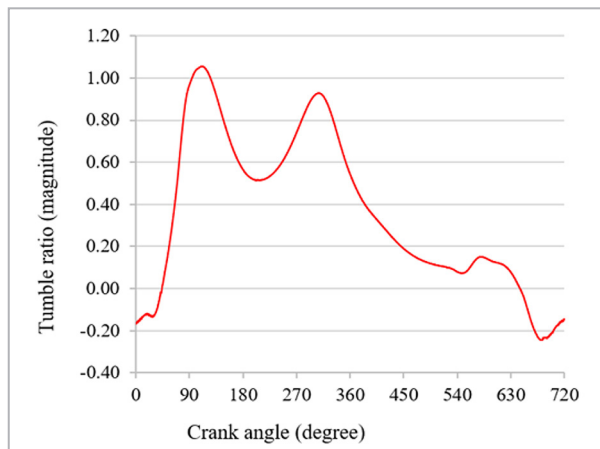


Figure 12 - Tumble ratio.

For comparison purposes, Figure 13 shows the magnitude and behavior of the

swirl and tumble ratio effects in the same graph as a function of the crank angle.

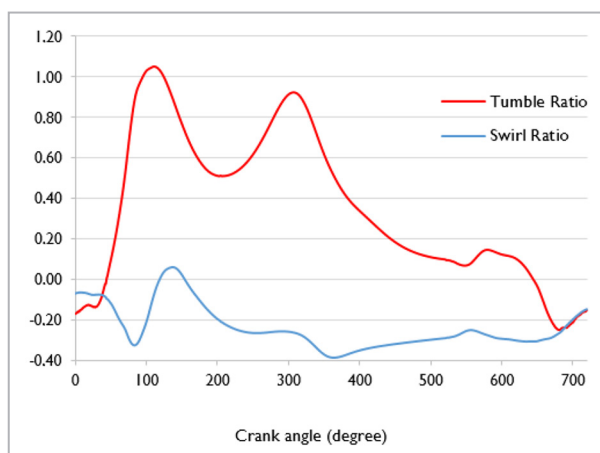


Figure 13 - Tumble and Swirl ratio.

To quantify the magnitude of the in-cylinder turbulent fluctuations during the engine cycle, the turbulence intensity was

determined with Equation 9. The graph shown in Figure 14 clearly presents a sharp increase for the turbulence intensity, which

is indicative of high-turbulence effects for the in-cylinder fluid intake up to 90°, as confirmed by Ferguson(2016).

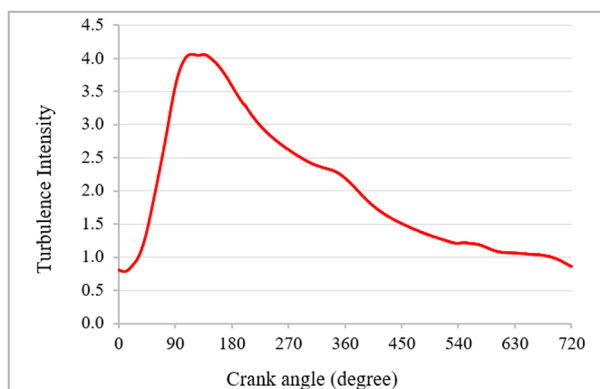


Figure 14 - Turbulence intensity.

Besides this, Ferguson (2016), also established a relationship between the turbulent intensity increase

and increasing swirl ratio. This can be seen when comparing Figures 11 and 14. In Figure 14, from 180° to 360°

(the compression stroke), a constant decrease can be seen until the end of the stroke, finishing with a high

turbulence intensity of 2.3. Following the cycle, a power stroke occurs from 360° to 540°, and the exhaust stroke takes place from 540° to 720°. In both

4. Conclusion

In this study, a dynamic mesh was used to simulate the model of a four-stroke internal combustion engine with a piston bowl. From the simulation results, it could be concluded that the proposed method is very innovative and perfectly capable of simulating the engine motion profile in cold flow, both accurately and realistically. This study also emphasizes the good properties of adaptability, quality and accuracy

cases the decrease is still visible and constant until it reaches a minimum value of approximately 0.9, characterizing, in this case, a small turbulence

intensity. This continuous decay is explained because of the low pressure and low temperatures applied in the simulations.

Acknowledgements

The authors are thankful for the support of the Universidade Federal de São João del-Rei (UFSJ) and Universidade Federal de Viçosa (UFV). This study was also carried out with financial

of results, because this special type of mesh was perfectly capable of satisfactorily dealing with the volume control of the engine during the entire engine cycle without having a single mesh problem. High quality levels were maintained when the dynamic mesh was analyzed under the orthogonal quality and skewness metrics, while providing excellent agreement when compared to experi-

mental results. Moreover, the excellent applicability to evaluate turbulence effects in engines was demonstrated, since they could be graphically illustrated and analyzed when considering the opening and closing of valves. These findings are usually adopted by researchers and engineers to intensify effects and enhance the performance and efficiency of internal combustion engines.

References

- ADDEPALLI, S. K.; MALLIKARJUNA, J. M. Parametric analysis of a 4-stroke GDI engine using CFD. *Alexandria Engineering Journal*, v. 57, p. 23-34, 2018. <http://dx.doi.org/10.1016/j.aej.2016.10.007>.
- ANSYS Inc. *User's guide*. Canonsburg, USA, 2013. (manuscrito não publicado).
- BASSE, N. T. Turbulence intensity scaling: a fugue. *Fluids*, v. 4, n. 4, 2018. DOI: 10.13140/RG.2.2.25385.13928.
- BLANCO, A. M.; ORO, J. M. F. Unsteady numerical simulation of an air-operated piston pump for lubricating greases using dynamic meshes. *Computers & Fluids*, v. 57, p. 138-150, 2012. DOI: 10.1016/j.compfluid.2011.12.014.
- BROATCH, A.; MARGOT, X.; GIL, A.; DONAYRE, J. C. Computational study of the sensitivity to ignition characteristics of the resonance in DI diesel engine combustion chambers. *Engineering Computation*, v. 24, n. 1, p. 77-96, 2007. DOI: 10.1108/02644400710718583.
- BRUNETTI, F. *Motores de combustão interna*. São Paulo: Edgard Blücher Ltda, 2012.
- CHUNG, T. J. *Computational fluid dynamics*. Cambridge University Press, Cambridge, UK, 2002.
- CONG, W.; LI, Z.; COA, K.; FENG, G.; CHENG, R. Transient analysis and process optimization of the spatial atomic layer deposition using the dynamic mesh method. *Chemical Engineering Science*, v. 217, 115513, 2020. <https://doi.org/10.1016/j.ces.2020.115513>.
- FERGUSON, C. R.; KIRKPATRICK, A. T. *Internal combustion engines: applied thermosciences*. 3. ed. Chichester, UK: John Wiley & Sons, 2016.
- GAFOOR, A. & GUPTA, R. Numerical investigation of piston bowl geometry and swirl ratio on emission from diesel engines. *Energy Conversion and Management*, v. 101, p. 541-551, 2015. Available in: <https://www.sciencedirect.com/science/article/pii/S0196890415005476?via%3Dihub>.
- GAO, X. W.; LIU, H.; CUI, M.; YANG, K.; PENG, H. Free element method and its application in CFD. *Engineering Computation*, v. 36, n. 8, p. 2747-2765, 2019. DOI: 10.1108/EC-10-2018-0471.
- GOSMAN, A. D. State of the art of multi-dimensional model of engine reacting flows. *Oil & Gas Science and Technology*, v. 54, n. 2, p. 149-159, 1999.
- HE, L.; ZHENG, J.; CHEN, J.; ZHENG, Y.; ZHOU, X.; XIAO, Z. Parallel algorithms for moving boundary problems by local remeshing. *Engineering Computation*, v. 36, n. 8, p. 2887-2910, 2019. DOI: 10.1108/EC-11-2018-0545.
- HUANG, R. F.; HUANG, C. W.; CHANG, S. B.; YANG, H. S.; LIN, T. W.; HSU, W. Y. Topological flow evolutions in cylinder of a motored engine during intake and compression stroke. *Journal of Fluids and Structures*, v. 20, p. 105-127, 2005. DOI: 10.1016/j.jfluidstructs.2004.09.002.
- ISLAM, A.; SOHAIL, M. U.; ALI, S. M.; HASSAN, A.; KALVIN, R. Simulation of four stroke internal combustion engine. *International Journal of Scientific & Engineering Research*, v. 7 n. 2, p. 1212-1219, 2016.
- JÚNIOR, F. V. Z. *Simulação numérica do escoamento turbulento em motores de combustão interna*, 2010. Available in: <http://hdl.handle.net/10183/25046>.
- KARTHIKEYAN, C. P.; SAMUEL, A. A.. CO₂-dispersion studies in an operation theatre under transient

- conditions. *Energy and Buildings*, v. 40, p. 231-239, 2008. DOI: 10.1016/j.enbuild.2007.02.023.
- KOZIEL, S.; TESFAHUNEGN, Y.; LEIFSSON, L. Variable-fidelity CFD models and co-Kriging for expedited multi-object aerodynamic design optimization. *Engineering Computation*, v. 33, n. 8, p. 2320-2338, 2016. DOI: 10.1108/EC-09-2015-0277.
- LAM, W. H.; ROBINSON, D. J.; HAMILL, G. A.; JOHNSTON, H. T. An effective method for comparing the turbulence intensity from LDA measurements and CFD predictions within a ship propeller jet. *Ocean Engineering*, v. 52, p. 105-124, 2012. <http://dx.doi.org/10.1016/j.oceaneng.2012.06.016>.
- LI, Z.; HARAMURA, Y.; KATO, Y.; TANG, D. Analysis of a high-performance model stirling engine with compact porous-sheets heat exchangers. *Energy*, v. 64, p. 31-43, 2014. <http://dx.doi.org/10.1016/j.energy.2013.11.041>.
- LIN, T. J.; GUAN, Z. Q.; CHANG, J. H.; LO, S. H. Vertex-ball spring smoothing: an efficient method for unstructured dynamic hybrid meshes. *Computers and Structures*, v. 136, p. 24-33, 2014. <http://dx.doi.org/10.1016/j.compstruc.2014.01.028>.
- MÚNERA, B. A. H.; ARRIETA, A. A. A.; SIERRA, F. J. C. Modelos para el estudio fenomenológico de la combustión sin llama con simulación numérica. *Ingeniería e Investigación*, v. 29, n. 2, p. 70-76, 2009.
- PRISCILLA & MEENA, P. A comprehensive study on in-cylinder IC engine due to swirl flow. *International Journal of Engineering Research & Technology*, v. 2, n. 7, p. 1156-1161, 2013.
- ROHITH, S.; PRAKASH, G. V. N. Cold flow simulation in an IC engine. *International Research Journal of Engineering and Technology*, v. 2, n. 7, p. 82-87, 2015.
- SHAFIE, N. A. M.; SAID, M. F. M. Cold flow analysis on internal combustion engine with different piston bowl configurations. *Journal of Engineering Science and Technology*, v. 12, n. 4, p. 1048-1066, 2017.
- SILVA, G. L. S.; CAMPOS, J. C. C.; SILVA, C. L. da; CARLOS, I. R. R.; SIQUEIRA, A. M. de O.; BRITO, R. F.; MINETTE, L. J. Flame temperature analysis in the oxycut process using acetylene gas: a numerical study. *The Journal of Engineering and Exact Sciences*, v. 6, p. 0555-0563, 2020. DOI: 10.18540/jcecvl6iss4pp0555-0563.
- WANG, C. et al. Progress in the CFD modeling of flow instabilities in anatomical total cavopulmonary connections. *Annals of Biomedical Engineering*, v. 35, n. 11, p. 1840-1856, 2007. DOI: 10.1007/s10439-007-9356-0.
- YIN, C.; ZHANG, Z.; SUN, T.; ZHANG, R. Effect of the piston top contour on the tumble flow and combustion features of a GDI engine with a CMCV: a CFD study. *Engineering Applications of Computational Fluid Mechanics*, v. 10, n. 1, p. 311-329, 2016.
- YOGESH, P.; KAILAS, D.; VIJAIYENDRA, P. In cylinder cold flow CFD simulation of IC engine using hybrid approach. *International Journal of Research n Engineering and Technology*, v. 8, p. 16-21, 2014.
- ZUNAID, M.; UPADHYAY, L.; GUPTA, N.; KUSHWAHA, S. Cold flow simulation for an IC engine with different lengths of connecting rod. *Journal of Mechanical and Civil Engineering*, v. 14, n. 1, p. 50-54, 2017. DOI: 10.9790/1684-1401075054.

Received: 1 February 2022 - Accepted: 13 July 2023.